ELSEVIER

Polymer 40 (1999) 2289–2301

polymer

Formation of anisotropic membranes via thermally induced phase separation

Hideto Matsuyama , Stephane Berghmans , Douglas R. Lloyd*

Department of Chemical Engineering, The University of Texas at Austin, Austin, TX 78712, USA

Received 12 May 1997; revised 16 December 1997; accepted 23 December 1997

Abstract

The applicability of the thermally induced phase separation (TIPS) process to the production of anisotropic membranes was investigated. To induce an anisotropic structure, diluent was evaporated from one side of the polymer–diluent melt-blended, thereby creating a concentration gradient in the nascent membrane prior to inducing phase separation. The system used to prepare these membranes was isotactic polypropylene (iPP) in diphenyl ether. The resulting membrane structures showed that this evaporation process was useful in producing anisotropic structures. The effects of evaporation time and initial polymer concentration on the anisotropic membrane structure were investigated. The evaporation process was analysed by solving appropriate mass transfer and heat transfer equations. The agreement between the calculated results and the experimental data on the membrane weight loss and the membrane thickness was satisfactory. The membrane structures are discussed in detail based on the calculated polymer volume fraction profiles in the membranes.

Keywords: Thermally induced phase separation; Anisotropic structure; Microporous membrane

1. Introduction

The thermally induced phase separation (TIPS) process is a valuable way of making microporous materials, such as membranes and foams [1–10] [11–20] [21–30]. In this process, a polymer is dissolved in a diluent at an elevated temperature. Upon removal of the thermal energy by cooling or quenching the solution, phase separation occurs. This can take the form of solid–liquid (S–L) TIPS, where the polymer crystallizes out of solution, or of liquid–liquid (L–L) TIPS, where the solution separates into a polymer-rich continuous phase and a polymer-lean droplet phase. A combination of these two processes is also possible.

In most previous studies on TIPS, isotropic structures have been produced; that is, the pore size did not vary across the thickness of the membrane. However, anisotropic membrane structures, with a gradation in pore size, are highly desirable for some microfiltration (MF) and/or ultrafiltration (UF) applications [31]. Compared with isotropic membranes with similar retention, anisotropic membranes show significant improvement in permeability and throughput. Wrasidlo reported the formation of highly anisotropic MF/UF membranes by the immersion precipitation process (wet phase inversion process) [32,33]. Anisotropic membranes can also be generated by the dry-cast process, although the degree of anisotropy obtained is not great [34,35].

Anisotropic and asymmetric (dense surface skin) membranes produced by TIPS have been reported [2,3,13,21,27,30]. The formation of the anisotropic or asymmetric structure was usually accomplished either by evaporation of diluent prior to phase separation [13,21,27,30] or by imposing a temperature gradient across the membrane during the quench process [2,3,13,21,27]. The presence of a skin due to evaporation often was unwanted and efforts had to be made to reduce evaporation in order to produce an anisotropic or isotropic membrane [27,30].

In this work, production of anisotropic or asymmetric TIPS membranes was achieved by inducing a polymer concentration gradient in the membrane solution prior to inducing phase separation. The concentration gradient was established by controlled evaporation of diluent from one side of the polymer–diluent solution at a temperature above the binodal. The evaporation induces a concentration gradient; the polymer concentration increases toward the top surface of the membrane. It is well known that the pore size of the membrane is dependent on the polymer concen-

* Corresponding author..

0032-3861/99/$ - see front matter
PII: S0032-3861(98)00040-8

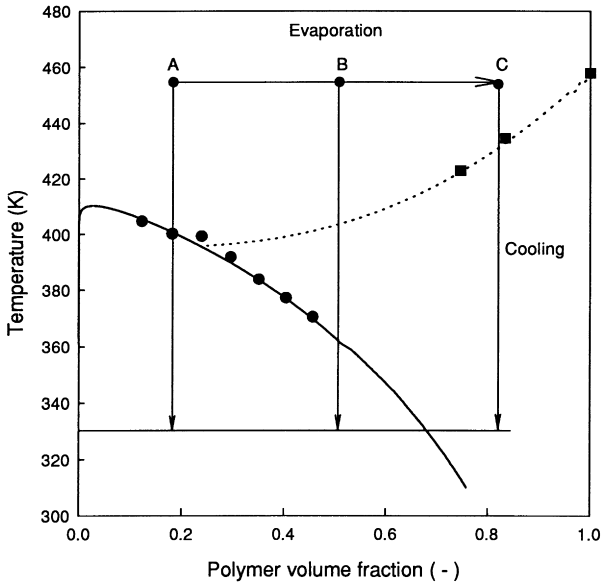

Fig. 1. Phase diagram for iPP/DPE system [23]: (●) cloud points; (■) experimental equilibrium melting points; (———) theoretical coexistence curve; (· · ·) theoretical melting point depression curve.

tration: the higher the polymer concentration, the smaller the pore size [13,23]. Thus, subsequent cooling of the membrane produces an anisotropic structure with smaller pores near the top of the membrane and larger pores near the bottom.

The effects of evaporation time and initial polymer concentration on membrane structure were investigated. Furthermore, the evaporation process was mathematically simulated. The calculated polymer volume fraction profiles in the solution prior to phase separation were used to understand the anisotropic membrane structures.

2. Background

Fig. 1 shows the phase diagram for the isotactic polypropylene (iPP)–diphenyl ether (DPE) system [23]. Point A represents the initial condition. When evaporation occurs only from the top surface on the melt-blend, the polymer volume fraction at the top surface increases to the value at point B, while the bottom surface volume fraction remains at point A. The sample is then cooled to induce phase separation, as shown by the arrows in Fig. 1. If the cooling rate is the same for both surfaces, the time spent in the binodal region for L–L separation is shorter for the top surface (from point B) than for the bottom (point A). There is less time for coarsening of the droplets generated by the phase separation in the higher polymer volume fraction region, which leads to smaller pores in the finished membrane. Even if coarsening time were similar, the higher polymer concentration (from point B) leads to slower droplet coarsening [36] owing to the higher viscosity of the polymer-rich matrix phase and lower volume fraction of the droplet phase.

If the polymer volume fraction at the top surface moves to point C, L–L phase separation may be preceded by S–L phase separation (polymer crystallization). In this case, the high polymer volume fraction at the top surface may produce a dense skin layer.

3. Analysis of the evaporation process

3.1. Mass transfer

Several models have been presented in the literature which analyse the evaporation step in a binary polymer solution; they were developed as a precursor for immersion precipitation and dry-cast processes [37–42]. The evaporation step is similar to that which precedes thermally induced phase separation, except for the operating temperatures. These models were used as a starting point for the model developed below.

A binary polymer–diluent system was used in this work. Since only the diluent evaporates from the solution, the diluent concentration decreases at the top (exposed) surface of the membrane solution, and the polymer concentration increases. The flux N_i relative to the stationary coordinate is given by

$$N_i = -\rho D_i\left(\frac{\partial w_i}{\partial z}\right) + \rho_i v \tag{1}$$

where ρ and ρ_i are the mass densities of the membrane solution and of component i, respectively. D_i and w_i denote the mutual diffusion coefficient and the weight fraction of component i, respectively. v is the mass average velocity. The mass transfer equations for the binary system are

$$\frac{\partial \rho}{\partial t} + \frac{\partial(\rho v)}{\partial z} = 0 \tag{2}$$

and

$$\frac{\partial \rho_2}{\partial t} + \frac{\partial(\rho_2 v)}{\partial z} = \frac{\partial}{\partial z}\left(\rho D_{23}\frac{\partial w_2}{\partial z}\right) \tag{3}$$

where subscripts 2 and 3 denote the diluent and polymer, respectively. t and z represent time and the position from the glass surface. D_{23} is the mutual diffusion coefficient of the diluent. Assuming no volume change on mixing,

$$\frac{1}{\rho} = \frac{w_2}{\rho_2^o} + \frac{w_3}{\rho_3^o} \tag{4}$$

where ρ_2^o and ρ_3^o are the pure diluent and polymer densities. From eqns (2), (3), (4), the following equation is derived in a manner similar to that used by Tan et al. [41]

$$v = -\left(\frac{1}{\rho_2^o} - \frac{1}{\rho_3^o}\right)\rho D_{23}\frac{\partial w_2}{\partial z} \tag{5}$$

The following mass transfer equation can be obtained via

substitution of eqn (5) into eqn (3)

$$\frac{\partial \rho_2}{\partial t} = \frac{\partial}{\partial z}\left(D_{23}\frac{\partial \rho_2}{\partial z}\right) \tag{6}$$

The initial and boundary conditions are

$$t = 0,\ \rho_2 = \rho_{20} \tag{7}$$

$$z = 0,\ \frac{\partial \rho_2}{\partial z} = 0 \tag{8}$$

$$z = L(t);\ \rho_{20}L_0 - \int_0^{L(t)} \rho_2\, \mathrm{d}z = \int_0^{\tau} k(\rho_{2g}^{i} - \rho_{2g}^{\infty})\, \mathrm{d}t \tag{9}$$

where $L(t)$ is the membrane thickness at time t, and k is the gas-side mass transfer coefficient. ρ_{20}, ρ_{2g}^{i} and ρ_{2g} are the initial mass density of the diluent in the cast solution, the mass density of the diluent in the gas phase at the air–film interface, and that in the gas bulk phase, respectively, can be expressed as follows when ideal gas behaviour on the air side is assumed and gas–liquid equilibrium is assumed at the air–film interface [39]

$$\rho_{2g}^{i} = \phi_2 \exp[1 - \phi_2 + \chi_{23}(1 - \phi_2)^2]\cdot\frac{P_2^o}{V_{2g}P} \tag{10}$$

where P and P_2^0 represent the total pressure and the pure diluent vapour pressure, respectively. V_{2g} is the partial specific volume of the diluent in the gas phase. ϕ_2 and χ_{23} are the volume fraction of the diluent and the diluent–polymer interaction parameter. The conservation equation for the polymer in the membrane solution is given by

$$\int_0^{L(t)} \rho_3\, \mathrm{d}z = L_0\rho_{30} \tag{11}$$

where subscript 0 denotes the initial value.

The membrane thickness decreases as time progresses in this system because of the evaporation of the diluent. The following coordination transformation was used to immobilize the interface position

$$\zeta = \frac{z}{L(t)} \tag{12}$$

This coordination transformation and the substitution of the volume fraction ϕ in place of the mass density ρ lead to the following equations

$$\frac{\partial \phi_2}{\partial t} = \frac{\zeta}{L(t)}\frac{\mathrm{d}L(t)}{\mathrm{d}t}\frac{\partial \phi_2}{\partial \zeta} + \frac{1}{L(t)^2}\frac{\partial}{\partial \zeta}\left(D_{12}\frac{\partial \phi}{\partial \zeta}\right) \tag{13}$$

$$t = 0;\ \phi_2 = \phi_{20} \tag{14}$$

$$\zeta = 0:\ \frac{\partial \phi_2}{\partial \zeta} = 0 \tag{15}$$

$$\zeta = 0;$$

$$\phi_{20}L_0 - L(t)\int_0^1 \phi_2\, \mathrm{d}\zeta = \int_0^{\tau} k\phi_2 \exp[(1 - \phi_2) + \chi_{23}(1 - \phi_2)^2]\left(\frac{V_2}{V_2 g}\right)\left(\frac{P_2^o}{P}\right)\mathrm{d}t \tag{16}$$

$$L(t) = \frac{L_0\phi_{10}}{\int_{\zeta=0}^{1} \phi_3\, \mathrm{d}\zeta} \tag{17}$$

where V_2 is the partial specific volume of the diluent in the liquid phase. In eqn (16), it is assumed that ρ_{2g} is negligibly small.

3.2. Heat transfer

The equation describing the heat transfer process is given by

$$\frac{\partial T}{\partial t} = \alpha\frac{\partial^2 T}{\partial z^2} \tag{18}$$

where α is the thermal diffusivity of the polymer solution. The initial and boundary conditions are

$$t = 0;\ T = T_0 \tag{19}$$

$$z = 0;\ T = T_0,\ \frac{\partial T}{\partial z} = 0 \tag{20}$$

$$z = L(t);\ K\frac{\partial T}{\partial z} = h(T_{\mathrm{gas}} - T) + \sigma\varepsilon(T_{\mathrm{gas}}^4 - T^4) - N_2\Delta H_2 \tag{21}$$

where K and h are the thermal conductivity of the polymer solution and the gas-side heat transfer coefficient, respectively. T_{gas} is the temperature in the gas bulk phase, σ and ϵ are the Stefan–Boltzmann constant and emissivity of the polymer solution, and ΔH_2 is the latent heat of evaporation of the diluent. Here, the temperature at the glass-facing surface is assumed to be equal to the initial temperature.

Applying the coordination transformation described in eqn (12) leads to

$$\frac{\partial T}{\partial t} = \frac{\zeta}{L(t)}\frac{\mathrm{d}L(t)}{\mathrm{d}t}\frac{\partial T}{\partial \zeta} + \frac{\alpha}{L(t)^2}\frac{\partial^2 T}{\partial \zeta^2} \tag{22}$$

$$t = 0;\ T = T_0 \tag{23}$$

$$z = 0;\ T = T_0,\ \frac{\partial T}{\partial \zeta} = 0 \tag{24}$$

$$\zeta = 1;\ \frac{K}{L}\frac{\partial T}{\partial \zeta} = h(T_{\mathrm{gas}} - T) + \sigma\varepsilon(T_{\mathrm{gas}}^4 - T^4) - N_2\Delta H_2 \tag{25}$$

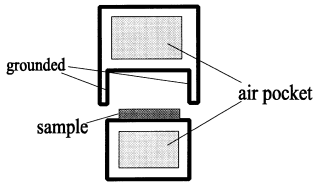

Fig. 2. Schematic diagram of glass bottle. The height of the space in the glass bottle was about 3 mm.

4. Experimental materials and method

The polymer and diluent used are isotactic polypropylene. (iPP, Himont Co., 6824PM) and diphenyl ether (DPE, Aldrich Chemical Co., 99% purity). All chemicals were used without further purification.

The preparation of a homogeneous polymer–diluent sample is similar to that described before [15]. Appropriate amounts of polymer and diluent were weighed into a test tube. The test tube was purged with nitrogen and sealed to prevent oxidation during melt-blending. The test tube was heated in an oven at the desired temperature for about 24 h, removed from the oven, and quenched in ice water to solidify the sample. The solid sample was chopped into small pieces. To make a solid sample with constant thickness, the small pieces were placed between a pair of microscope cover slips with a Teflon spacer inserted between the two cover slips. This sample assembly was heated again to cause melt-blending and was then cooled to room temperature. The resulting solid sample was measured in different places and found to have an average thickness of 600 μm (± 10%).

After putting the solid polymer–diluent sample in the glass bottle shown in Fig. 2, the sample was sealed and heated to 433.2 K to cause melt-blending. The glass cap was then taken off and evaporation of diluent was allowed from the exposed (air-facing) surface into the air at 433.2 K, thereby creating a polymer concentration gradient in the sample. After evaporation for the desired time, the glass cap was replaced and the entire assembly was removed from the oven and slowly cooled in 298 K air.

Diphenyl ether was extracted from the membrane by immersing it in methanol overnight. Methanol was then allowed to evaporate from the resulting microporous structure. The final sample was immersed in liquid nitrogen, fractured and coated with gold–palladium using a sputtering coater (Commonwealth Model 3, Pelco). The cross section of the membrane was viewed using a scanning electron microscope (JOEL JSN-35C) under an accelerating voltage of 25 kV. The thickness of the samples was measured before and after extraction.

Table 1
Parameters used in eqn (26).

V^*_2 ($cm^3\ g^{-1}$)[a]	0.506
V^*_3 ($cm^3\ g^{-1}$)[a]	1.034
ξ[b]	1.18
D_{02} ($cm^2\ s^{-1}$)[c]	2.36×10^{-4}
$K_{12\gamma}$ (cm^3 (g K)$^{-1}$)[c]	8.34×10^{-4}
$K_{22} - T_{g2}$ (K)[c]	− 142.0
K_{13}/γ (cm^3 (g K)$^{-1}$)[d]	4.99×10^{-4}
K_{23} (K)[d]	2.27×6
T_{g3} (K)[e]	257

[a] V^*_2 and V^*_3 were estimated as the specific volumes of the diluent and polymer at 0 K, which can be obtained using group contribution methods [45,47]. [b] $x = M_2V^*_2/V_{2j}$ [45] (M_2 is the molecular weight of diluent; V_{2j} is the molar volume of polymer jumping unit). V_{2j} was estimated by the equation of V_2j = O.6224T_{g3} − 86.95 [45]. [c] These values were determined by Dullien's equation [45] based on viscosity data [48] for the pure diluent on the assumption of negligible energy effects ($E = 0$). [d] These values were determined by WLF equations [45]. The polymer WLF parameters at 433.2 K were estimated from average values at glass transition temperature available in Ref. [49]. [e] Ref. [50]

5. Results and discussion

5.1. Analysis of evaporation process

To simulate the evaporation process using eqns (13), (14), (15), (16), (17) and eqns (22), (23), (24), (25), several parameters must be determined. The diffusion coefficient based on the free volume theory by Vrentas and Duda [43–46] was used as D_{23} in eqn (13). According to this theory, the self-diffusion coefficient D^*_2 and D_{23} are expressed as

$$D_{23} = D^*_2(1 - \phi_2)^2(1 - 2\chi_{23}\phi_2) \tag{26}$$

$$D^*_2 = D_{02}\exp\left(\frac{-E}{RT}\right) \times \exp\left(\frac{-(\omega_2 V^*_2 + \omega_3 \xi V^*_3)}{\omega_2 \frac{K_{12}}{\gamma}(K_{22} - T_{g2} + T) + \omega_3 \frac{K_{23}}{\gamma}(K_{23} - T_{g3} + T)}\right) \tag{27}$$

where, V^*_i is the specific critical hole free volume of component i required for a jump, w_i is the weight fraction of component i, and T_{gi} is the glass transition temperature of component i. D_{02} is the pre-exponential factor of the diluent, E is the energy per mole that a molecule needs to overcome attractive force, and γ is the overlap factor, which is introduced because the same free volume is available to more than one molecule. Parameter ξ is the ratio of the critical molar volumes for the diluent and polymer jumping units. K_{12} and K_{22} are free-volume parameters for the diluent, while K_{13} and K_{23} are those for the polymer.

All parameters except χ_{23} were estimated according to Zielinski and Duda's method [45]. The interaction parameter χ_{23} for the iPP–DPE system is given by McGuire [23] as

$$\chi_{23} = -1.40 + \frac{792}{T} \tag{28}$$

Table 2
Parameters used in the estimation of k and h, and the analysis of the evaporation.

D_{2g} ($cm_2\ s^{-1}$)[a]	0.107
μ_g (Pa S)[b]	2.44×10^{-5}
ρ_g (g cm^{-3})[c]	8.15×10^{-4}
η[d]	− 4.88
L_c (cm)[e]	0.6
K_g (W (m K)$^{-1}$)[b]	0.0148
C_{pg} (J (g K)$^{-1}$)[b]	1.017
β (K^{-1})[d]	2.31×10^{-3}
P_2^0 (mmHg)[f]	exp(18.4 − 6226/T)
V_{2g} ($cm^3\ g^{-1}$)[d]	209
ΔH_2 (J mol^{-1})[g]	5.48×10^{-8}
σ (J (m^2 s K^4)$^{-1}$)	5.67×10^{-8}
ϵ[h]	0.81
K_2 (W (m K)$^{-1}$)[i]	0.131
K_3 (W (m K)$^{-1}$)[j]	0.237
C_{p2} (J (g K)$^{-1}$)[i]	1.58
C_{p3} (J (g K)$^{-1}$)[k]	5.80
ρ_2 (g cm^{-3})[l]	0.9597
ρ_3 (g cm^{-3})[m]	0.850

[a]Estimated from Chapman–Enskog equation [52]. [b]Value for air [48]. [c]Value for air [53]. [d]Calculated by assuming the ideal gas. [e]Hydraulic diameter of melt-blending sample. [f]Two parameters in this Clapeyron equation were determined from two vapour-pressure points [53]. [g]Estimated by the following equation given by Reid *et al.* [54] p. 467: $\Delta H_2 = Rt_c[7.08(1 - T_r)^{0.354} + 10.95\omega_2(1 - T_r)^{0.456}]$ where T_c = critical temperature, T_r = reduced temperature, ω_2 = acentric factor of diluent. [h]Ref. [40]. [i]Refs [55], p. 458. [j]Ref. [56]. [k] Ref. [57]. [l]The density at 433 K was estimated by using the following equation [53]: $r = P_c/(RT_cZ_{RA}^{\{1+(1-Tr)2/7\}})$ (P_c = critical pressure, Z_{RA} = constant determined from experimental data). [m] Ref. [58].

Therefore, no fitting parameters were used to calculate D_{23}. The parameters used in eqn (26) are listed in Table 1.

The gas-side mass transfer coefficient k and gas-side heat transfer coefficient h were estimated by eqns (29), (32)[51], respectively because the evaporation process was carried out under almost free convection conditions. In eqns (29), (32), the coefficient of 0.54 was used because the experimental condition in this work corresponds to the case of a heated plate facing up [51].

$$kL_c y_{air}^{lm}/D_{2g} = 0.54(Gr^m Sc)^{0.25} \tag{29}$$

$$Gr^m = L_c^3 \rho_g^2 g[\eta(y_{2g}^i - y_{2g}^\infty)]/\mu_g^2 \tag{30}$$

$$Sc = \mu_g/(\rho_g D_{2g}) \tag{31}$$

$$hL_c/K_g = 0.54(Gr^h Pr)^{0.25} \tag{32}$$

$$Gr^h = L_c^3 \rho_g^2 g\beta\Delta t/\mu_g^2 \tag{33}$$

$$Pr = C_{pg}\mu_g/K_g \tag{34}$$

Here, L_c and y_{air}^{1m} denote the characteristic length of the cast film surface and the logarithm mean mole fraction difference of air. D_{2g}, ρ_g and μ_g are the mutual diffusion coefficient of the diluent in the gas phase, total mass density of the gas phase, and viscosity of the gas, respectively. y^i_{2g} and y_{2g} are the mole fraction of the diluent at the air–film interface and that in the gas bulk phase. g is the gravity constant and coefficient η is given by $-(1/\rho_g)(\partial\rho_g/\partial y_{2g})_{P,T}$. K_g and C_{pg} are the thermal conductivity and heat capacity of gas phase. Δt is the temperature difference between the air–film interface and the gas bulk phase, and coefficient β is given by $(1/V)(\partial V/\partial T)_P$. Gr^m and Gr^h are Grashof numbers for mass transfer and for heat transfer. Sc and Pr are the Schmidt and Prandtl numbers. The parameters used for the calculation of k and h are summarized in Table 2 along with other parameters.

The thermal diffusivity of the polymer solution α was estimated by

$$\alpha = \frac{\phi_2 K_2 + (1 - \phi_2)K_3}{[\phi_2 C_{p2} + (1 - \phi_2)C_{p3}][\phi_2\rho_2 + (1 - \phi_2)\rho_3]} \tag{35}$$

Fig. 3 shows polymer concentration profiles across the thickness of the membrane for periods of evaporation ranging from zero to 6 min. The polymer volume fraction at the top surfaces increases as evaporation continues; the concentration at the bottom surface remains unaffected for at least 4 min. Evaporation leads to a concentration gradient in the nascent membrane and a decrease in membrane thickness with increased evaporation time, as shown.

Fig. 4 shows the same polymer volume fraction profiles as above, over a range of dimensionless position where the top surface is defined to be 1.0 (see eqn (12)). Profiles for three different initial polymer volume fractions are shown. The evaporation rate increases as the initial polymer concentration decreases. This rate increase results in anisotropy across a larger portion of the membrane for lower concentrations. The profiles for the 15 wt% sample show this clearly; the concentration profiles extend more deeply into the membrane than the corresponding profiles for the 20 and 30 wt% samples. This trend is more clearly shown in

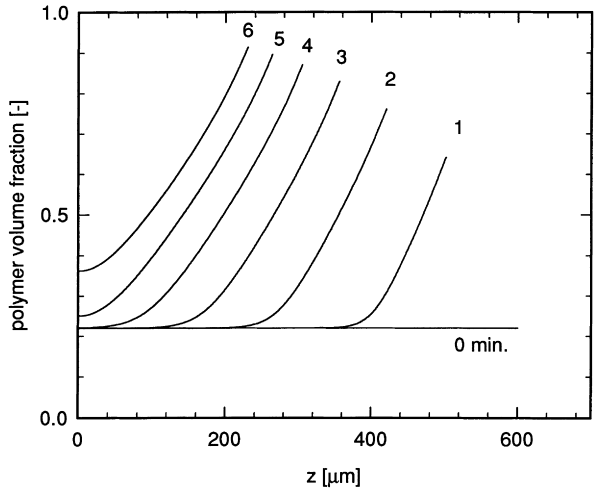

Fig. 3. Calculated polymer volume fraction profiles *versus* cross-sectional position; zero is bottom surface of membrane. Sample: 2O wt% iPP.

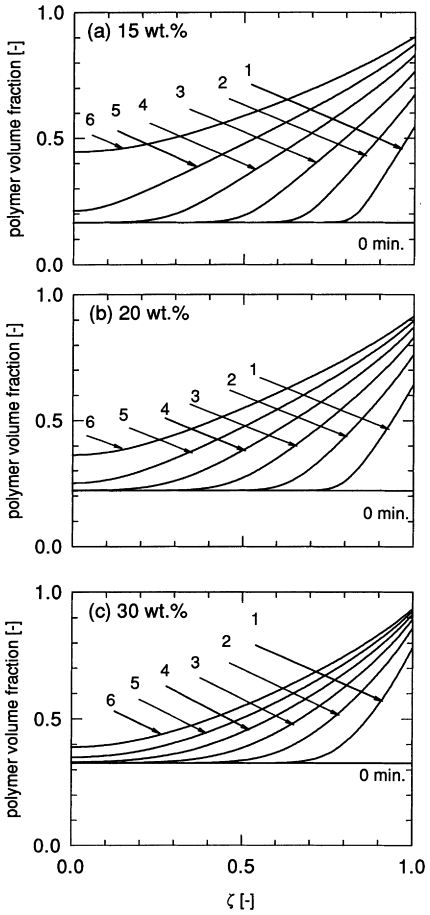

Fig. 4. Polymer volume fraction profiles *versus* dimensionless position; zero is bottom surface, 1.0 is top surface. (a) 15 wt% iPP sample; (b) 2O wt% iPP sample; (c) 3O wt% iPP sample.

Fig. 5, where the polymer volume fractions at the top and bottom surfaces are plotted against evaporation period.

Fig. 6 shows the change in the calculated temperature at the top surfaces for the case of evaporation into air at 433.2 K. The temperature initially decreases owing to heat

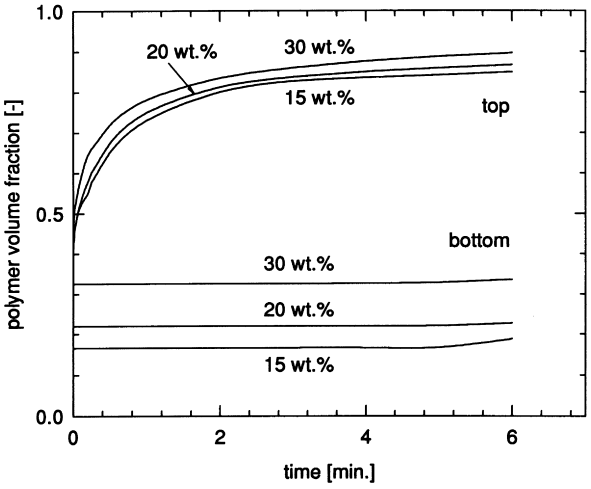

Fig. 5. Polymer volume fractions at top and bottom surfaces *versus* time.

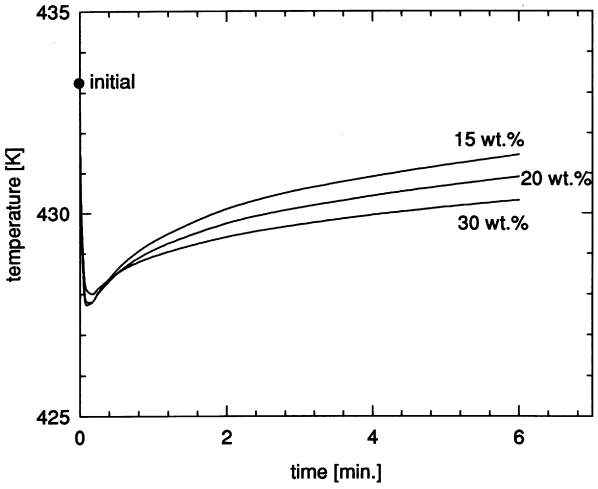

Fig. 6. Temperature at top surface *versus* time.

loss through evaporation of diluent. The temperature reaches a minimum when convective and radiative heat transfer from the surrounding atmosphere to the nascent membrane balance the heat loss through evaporation. The evaporation rate decreases owing to a decrease in the diffusion coefficient, and to a lower temperature which also decreases the evaporation rate. The atmosphere puts energy back into the system, gradually raising the surface temperature back near the initial (and atmospheric) temperature. The temperature changes during the evaporation process

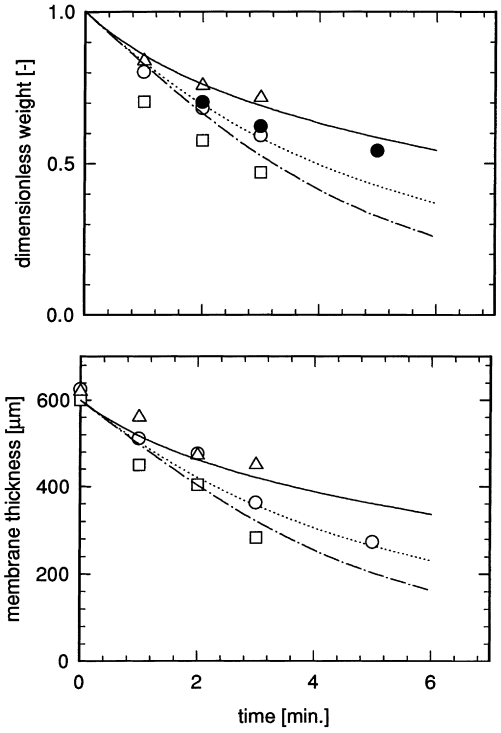

Fig. 7. Dimensionless weight and thickness changes over time: □, 0:15 wt% iPP; ○, ●, 20 wt% iPP; △, 30 wt% iPP; — – —, 15 wt% iPP; · · ·, 20 wt% iPP; ———, 30 wt% iPP.

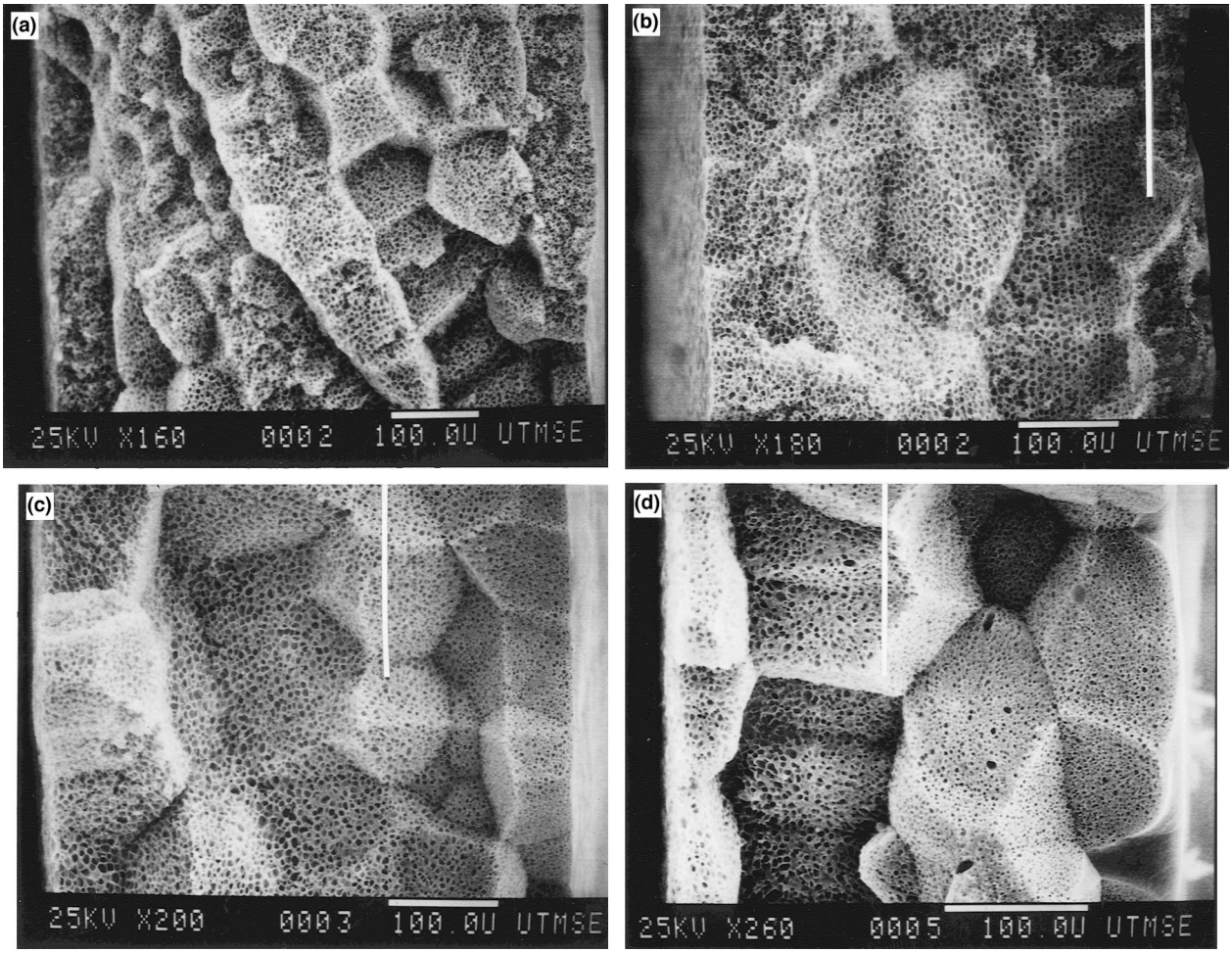

Fig. 8. Micrograph of the cross sections of 2O wt% sample: (a) evaporation time = 0; (b) evaporation time = 1 min; (c) evaporation time = 2 min; (d) evaporation time = 3 min. The right and left sides correspond to the top and bottom surfaces, respectively.

are within 7 K, not a significant drop compared with the initial temperature of 433.2 K.

A comparison of the calculated results and the experimental data for the dimensionless membrane weight and membrane thickness are shown in Fig. 7. The dimensionless membrane weight is defined as the weight after evaporation divided by the initial weight. The membrane thicknesses were measured after cooling the solution to induce phase separation and extracting the diluent by methanol. The open circles (○) and filled circles (●) are data from different experiments with the same sample (20 wt%). The agreement between data indicates the good reproducibility of these experiments. For lower initial polymer concentrations, the diffusion coefficient of the solution will be higher; there is a correspondingly higher evaporation rate and a higher weight and thickness loss over the same time period. The lines representing the calculated results for both the dimensionless weights and the membrane thicknesses show reasonable agreement with the experimental data. The agreement between the calculated results and the experimental data on the membrane thickness suggests that the membrane thickness does not change appreciably over the course of phase separation and extraction, since the model calculates thickness prior to phase separation and experimental measurement takes place after extraction of the diluent.

5.2. Membrane structures

Fig. 8 shows the cross sections of the membranes obtained for the different evaporation times. Each figure shows that microporous spherulites are formed, owing to the crystallization of iPP. Fig. 9 shows the cross sections at higher magnification, focusing near the top and bottom surfaces. Twenty weight% iPP/DPE samples were used for all of these membranes. In all cases, cellular pore structures were observed, which is characteristic of a polymer mixture undergoing liquid–liquid TIPS. Therefore, the phase separation process in this case is liquid–liquid phase separation with subsequent polymer crystallization [59]. In the case of no evaporation, the membrane structure was almost isotropic (Fig. 8a) with the pore size at the bottom surface ($\sim$ 5.0 μm) nearly equal to that at the top surface (see Fig.

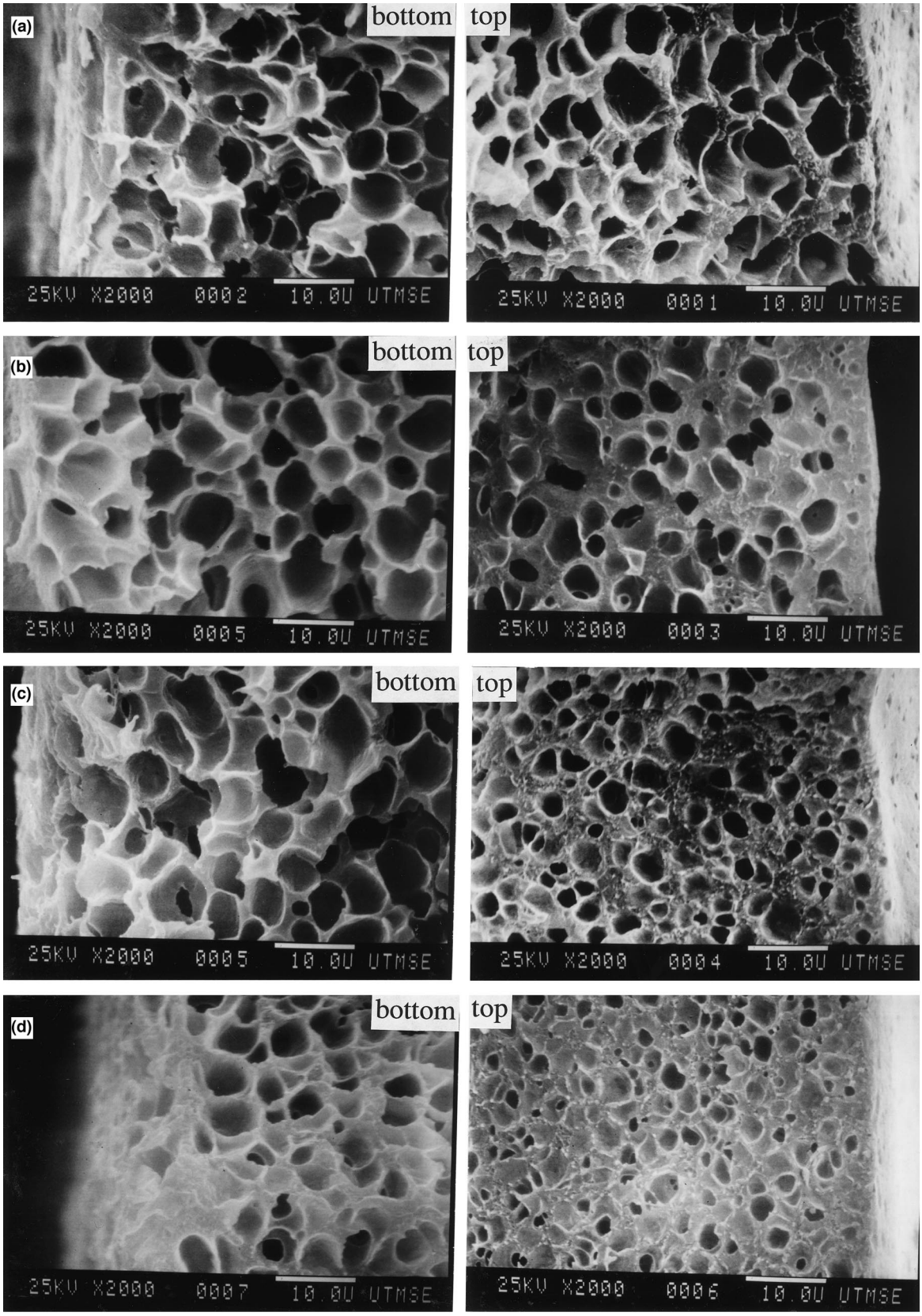

Fig. 9. Detail structures at top and bottom surfaces for 2O wt% sample: (a) evaporation time = 0; (b) evaporation time = 1 min; (c) evaporation time = 2 min; (d) evaporation time = 3 min.

Table 3
Comparison of positions of boundary of changes in pore sizes with calculated positions at which polymer volume fractions start to increase

Evaporation time	1 min	2 min	3 min
15 wt% sample			
Approximate observed boundary position	0.8	0.6	0.5
Position where polymer volume fraction starts to increase	0.79	0.62	0.43
20 wt% sample			
Approximate observed boundary position	0.9	0.7	0.4
Position where polymer volume fraction starts to increase	0.74	0.55	0.36
30 wt% sample			
Approximate observed boundary position	0.8	0.5	0.3
Position where polymer volume fraction starts to increase	0.66	0.44	0.26

9a). This result indicates that the cooling rates at both surfaces were nearly equal.

On the other hand, as the evaporation time increases, anisotropic structures were formed (Fig. 8b–d). The gradient from the smaller pores at the top surface to larger pores at the bottom surface is caused not by the difference in the cooling rates, but by the polymer concentration gradient induced by the evaporation. The difference in the pore sizes between top and bottom surfaces is more clearly shown in Fig. 9b–d. These experimental results indicate that anisotropic structures can be successfully obtained by introducing an evaporation process before the temperature quenching step. As shown in Fig. 8b–d, the beginning of anisotropy, where pore size begins to decrease, is closer to the bottom of the membrane for increased evaporation time. A careful visual inspection of the micrographs allows one to estimate this beginning of anisotropy; a white line is drawn to represent the approximation. Spherulitic structure obscures the boundary somewhat, and is a possible source of error. The observed beginnings of anisotropy for varying initial polymer concentrations and evaporation times have been summarized in Table 3. Model calculation results for the same conditions, obtained from Fig. 4, have been included for comparison. The table shows that there is

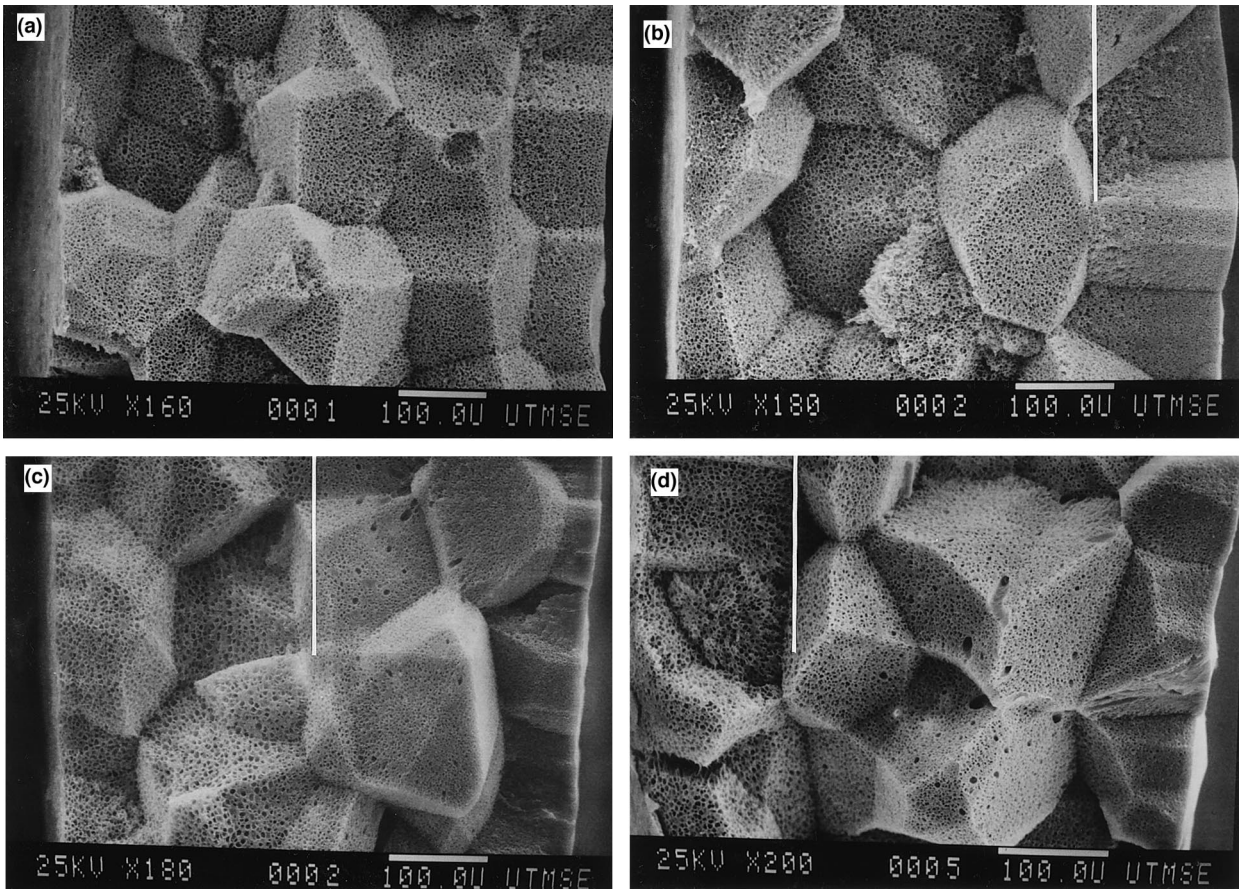

Fig. 10. Micrograph of the cross sections of 3O wt% sample: (a) evaporation time = 0; (b) evaporation time = 1 min; (c) evaporation time = 2 min; (d) evaporation time = 3 mm. The right and left sides correspond to the top and bottom surfaces, respectively.

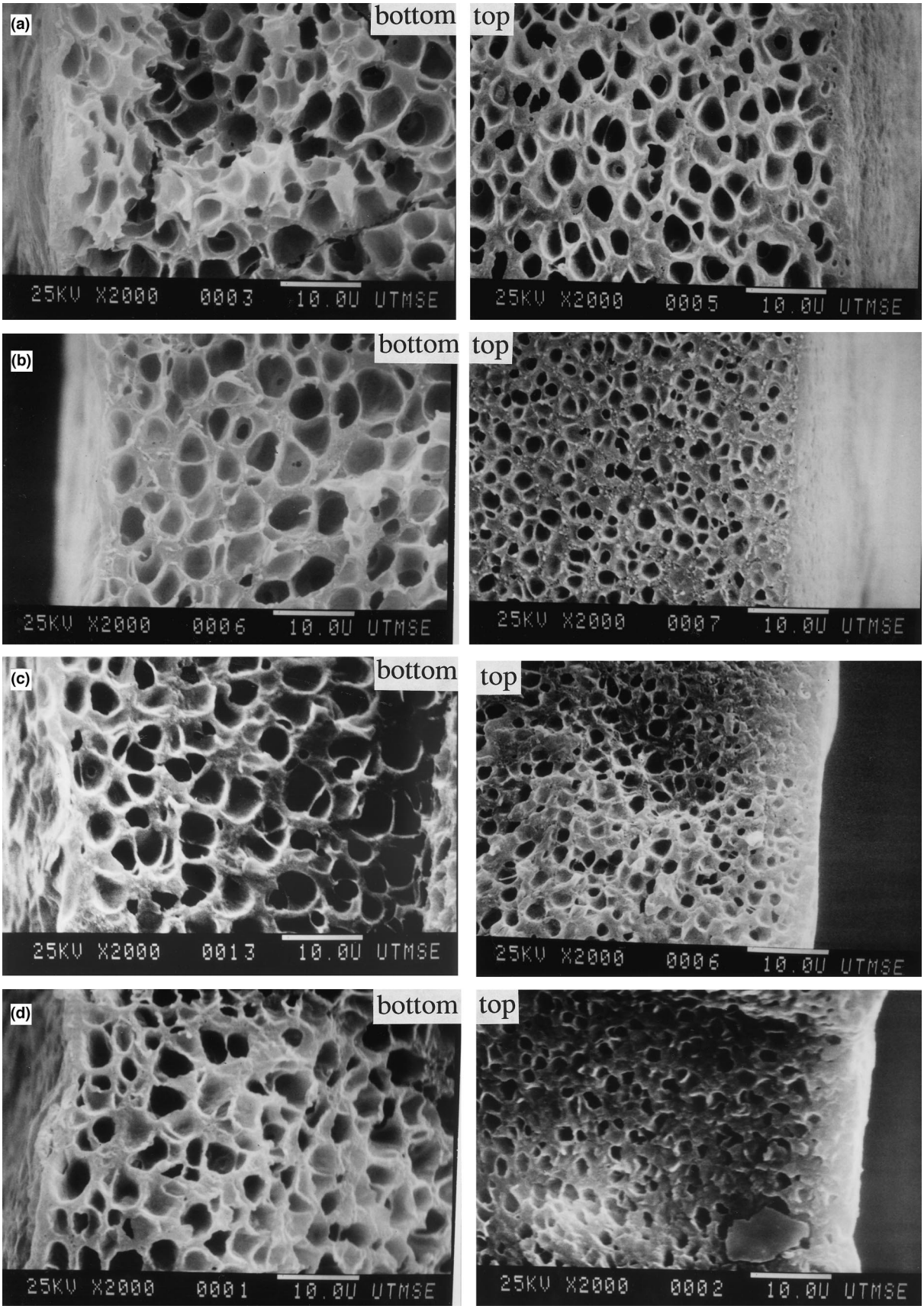

Fig. 11. Detail structures at top and bottom surfaces for 3O wt% sample: (a) evaporation time = 0; (b) evaporation time = 1 min; (c) evaporation time = 2 min; (d) evaporation time = 3 min.

approximate agreement between experimental and model results, which is a measure of the model's validity.

The pore size near the bottom surface remained virtually unchanged over the range of 1–3 min evaporation time, as shown in Fig. 9b–d. This is in agreement with the calculated results in Fig. 4, where the polymer concentration near the bottom surface is equal to the initial concentration for evaporation times of up to 4 min. Near the top surface, the pore size decreases as evaporation time increases (Fig. 9b–d). This observation corresponds to the increase in polymer concentration at the top surface predicted by the model, as shown in Fig. 4.

It is possible that anisotropy is also occurring in the formation of spherulites across the thickness of the membrane; evidence of this was not clear. There are not enough spherulites spanning the membrane cross section to draw a conclusion.

Figs 10–13 show the membrane structures for 30 and 15 wt% iPP–DPE samples, respectively. Once again in the cases of no evaporation, nearly isotropic structures were obtained for both samples. The pore sizes obtained were $\sim 3.5\ \mu m$ for the 30 wt% sample and $\sim 6.5\ \mu m$ for the 15 wt% sample. The pore size for the 20 wt% sample already discussed was $\sim 5.0\ \mu m$. These results coincide with previous observations that higher initial polymer concentration results in smaller pore size [21,23]. For both the 30 and 15 wt% samples, evaporation of the diluent produced anisotropic structures. The degree of anisotropy, which is defined as the ratio of pore diameters in the two surfaces [31], was about 8 in the case of Fig. 11d. As shown in Figs 11 and 13, the pore sizes at the bottom surfaces did not change, which again agrees with the calculated results in Fig. 4. Furthermore, the pore sizes at the top surface decreases with increased evaporation time for all weight fractions; and a skin layer of approximately 2 μm thickness was formed on the top surface in the 30 wt% system with 3 min evaporation time. This indicates that the evaporative TIPS process is capable of producing an asymmetric structure.

6. Conclusions

Anisotropic structures were successfully obtained by the TIPS process by introducing an evaporation step before the temperature quenching. Evaporation from one side of the melt blended solution induced a polymer concentration gradient in the membrane, which led to smaller pores at the top surface. In the case of no evaporation, nearly isotro-

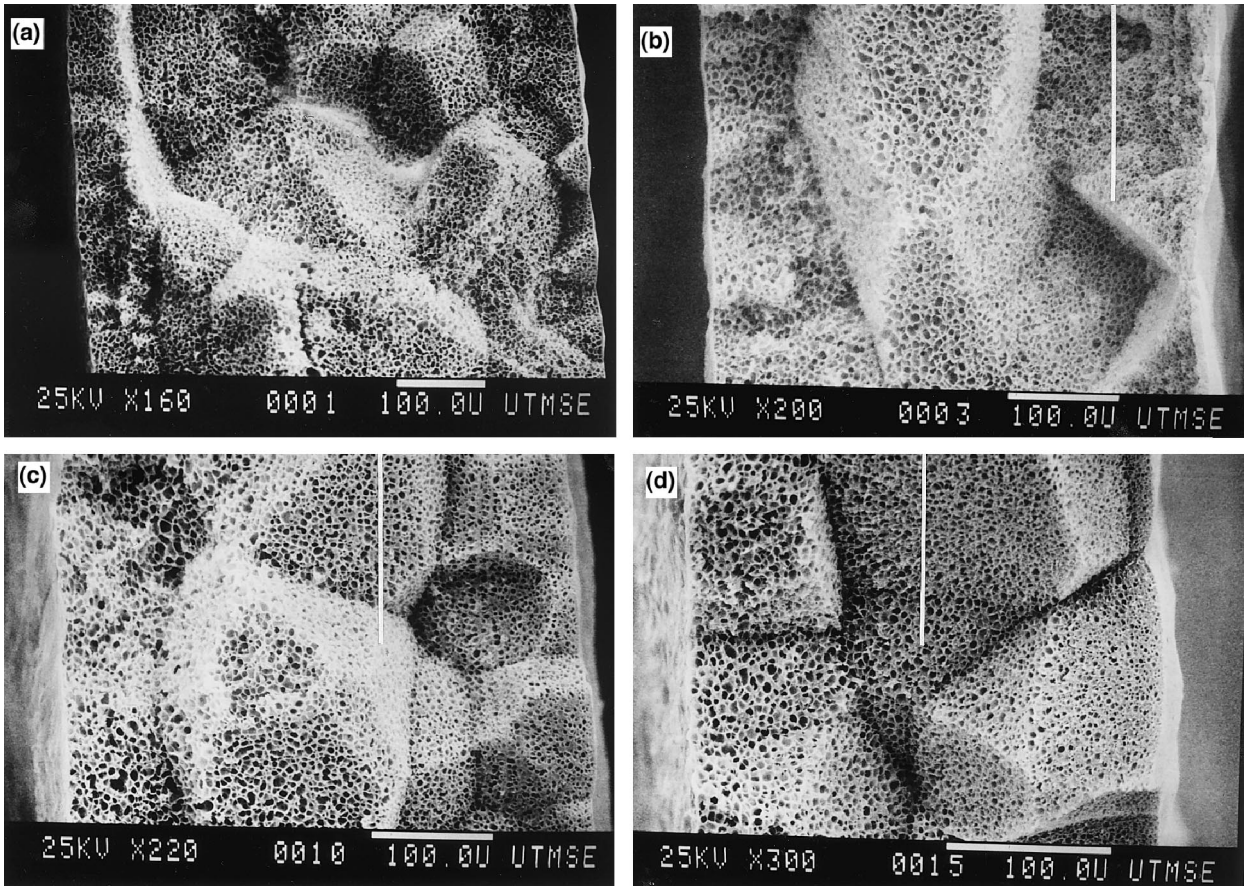

Fig. 12. Micrograph of the cross sections of 15 wt% sample: (a) evaporation time = 0; (b) evaporation time = 1 min; (c) evaporation time = 2 min; (d) evaporation time = 3 min. The right and left sides correspond to the top and bottom surfaces, respectively.

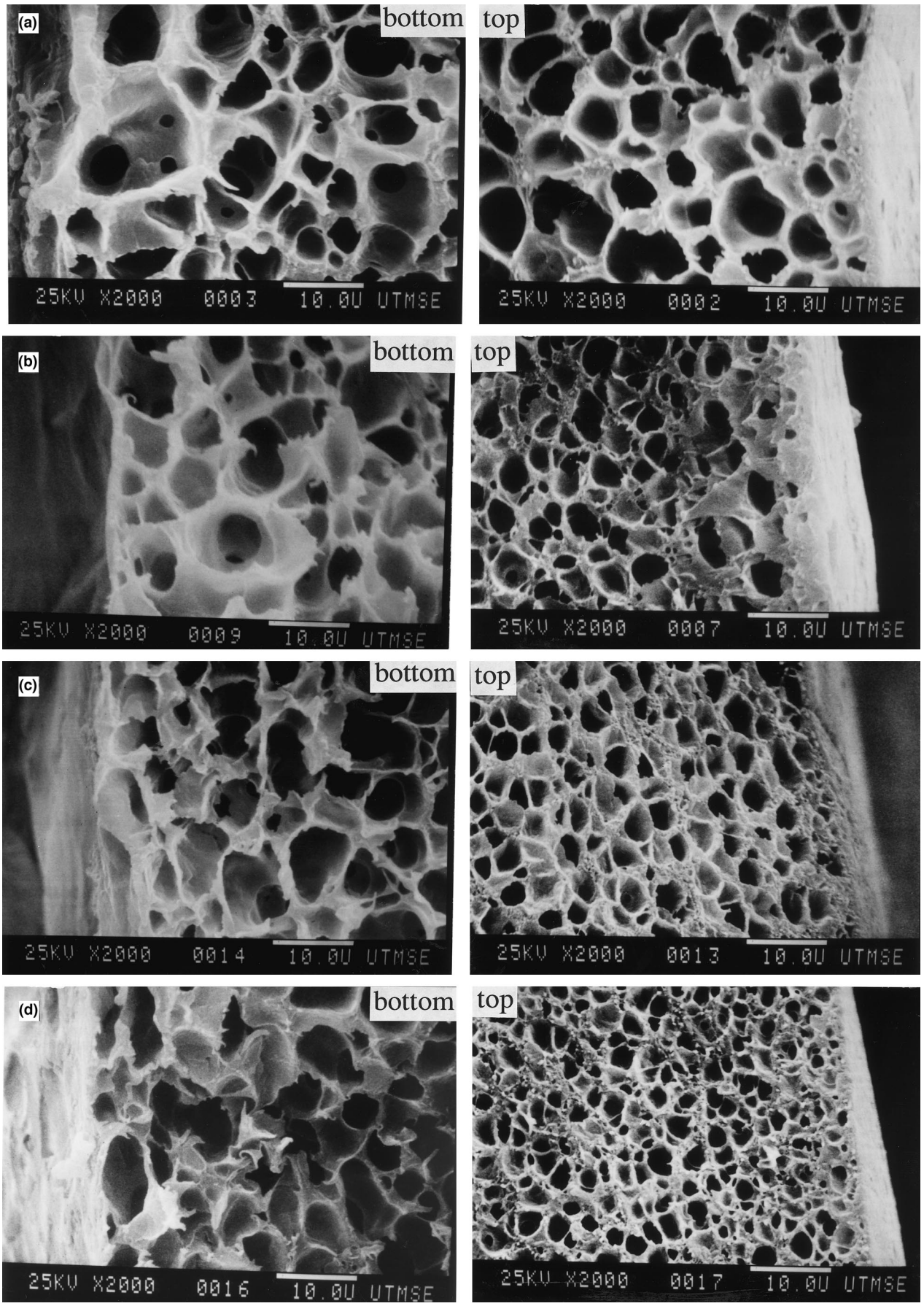

Fig. 13. Detail structures at top and bottom surfaces for 15 wt% sample: (a) evaporation time = 0; (b) evaporation time = 1 min; (c) evaporation time = 2 min; (d) evaporation time = 3 min.

pic structures were obtained. This indicates that the cooling rates at both surfaces were controlled to be nearly equal in this set of experiments. As the evaporation time increased, the position of the boundary between pores influenced by evaporation (small pores) and pores unaffected by evaporation (large pores) shifted to greater depths in the membrane cross section. Also, the pore size at the top surfaces decreased while the pore size at the bottom surface was unchanged by increased evaporation time. In the case of 30 wt% iPP in DPE, an asymmetric structure with a skin layer on the top surface was formed for the longer evaporation times.

The evaporation process was simulated by solving the appropriate mass transfer and heat transfer equations, and calculating the concentration profiles during the evaporation step. The calculated membrane weight and thickness loss due to evaporation were in approximate agreement with the experimental results. There was also satisfactory agreement between the experimentally observed and calculated beginning of anisotropy.

References

[1] Castro AJ. US Patent 4,247,498, 1981.
[2] Caneba GT, Soong DS. Macromolecules 1985;18:2538.
[3] Caneba GT, Soong DS. Macromolecules 1985;18:2545.
[4] Hiatt WC, Vitzthum GH, Wagener KB, Gerlach K, Josefiak C. In: Lloyd DR, editor. Materials science of synthetic membranes, ACS Symposium Series, 269. Washington, DC: American Chemical Society, 1985:229.
[5] Aubert JH, Clough RL. Polymer 1985;26:2047.
[6] Schaaf P, Lotz B, Wittmann JC. Polymer 1987;28:193.
[7] Williams JM, Moore JE. Polymer 1987;28:1950.
[8] Hikmet RM, Callister S, Keller A. Polymer 1988;29:1378.
[9] Aubert JH. Macromolecules 1988;21:3468.
[10] Lloyd DR, Barlow JW, Kinzer KE. In: Sirkar KK, Lloyd DR, editors. New membrane materials and processes for separation, AIChE Symposium Series 261. New York: American Institute of Chemical Engineers, 1988.
[11] Williams JM, Moore JE. Polymer 1989;30:2279.
[12] Lloyd DR, Kim SS, Kinzer KE. Journal of Membrane Science 1991;64:1.
[13] Tsai F-J, Torkelson JM. Macromolecules 1990;23:775.
[14] Lloyd DR, Kinzer KE, Tseng HS. Journal of Membrane Science 1990;52:239.
[15] Kim SS, Lloyd DR. Journal of Membrane Science 1991;64:13.
[16] Lim GBA, Kim SS, Ye Q, Wang YF, Lloyd DR. Journal of Membrane Science 1991;64:31.
[17] Alwattari AA, Lloyd DR. Journal of Membrane Science 1991;64:55.
[18] Vandeweerdt P, Berghmans H, Tervoort Y. Macromolecules 1991;24:3547.
[19] McGuire KS, Lloyd DR, Lim GBA. Journal of Membrane Science 1993;79:27.
[20] Vadalia HC, Lee HK, Myerson AS, Levon K. Journal of Membrane Science 1994;89:37.
[21] Berghmans S, Mewis J, Berghmans H, Meijer HEH. Polymer 1995;36:3085.
[22] Li W, Yuan Y, Cabasso I. Chinese Journal of Polymer Science 1995;13:7.
[23] McGuire KS. Membrane formation via liquid–liquid thermally induced phase separation. Dissertation, The University of Texas at Austin, 1995.
[24] Song S-W, Torkelson JM. Journal of Membrane Science 1995;98:209.
[25] Mehta RH, Madsen DA, Kalika DS. Journal of Membrane Science 1995;107:93.
[26] Kim J-J, Hwang JR, Kim UY, Kim SS. Journal of Membrane Science 1995;108:25.
[27] Berghmans S. Spinning of hollow porous fibres. Dissertation, K.U. Leuven, 1995.
[28] Berghmans S, Berghmans H, Meijer HEH. Journal of Membrane Science 1996;116:171.
[29] Chiang C-Y, Lloyd DR. Journal of Porous Materials 1996;2:273.
[30] Caplan MR, Chiang CY, Lloyd DR, Yen LY. Journal of Membrane Science 1997;130:219.
[31] Zeman LJ, Zydney AL. Microfiltration and ultrafiltration. New York: Marcel Dekker, 1996.
[32] Wrasidlo WJ, Mysels KJ. J Parenteral Sci Technol 1984;38:24.
[33] Wrasidlo WJ. US Patent 4,629,563, 1986.
[34] Kesting RE, Murrag A, Newmann J. Pharm Tech 1981;18:2538.
[35] Zeman L, Fraser T. Journal of Membrane Science 1994;87:267.
[36] McGuire KS, Laxminarayan A, Lloyd DR. Polymer 1995;36:4951.
[37] Castellari C, Ottani S. Journal of Membrane Science 1981;9:29.
[38] Krantz WB, Ray RJ, Sani RL, Gleason KJ. Journal of Membrane Science 1986;29:11.
[39] Tsay CS, McHugh AJ. Journal of Membrane Science 1991;64:81.
[40] Shojaie SS, Krantz WB, Greenberg AR. Journal of Membrane Science 1994;94:255.
[41] Tan L, Krantz WB, Greenberg AR, Sani RL. Journal of Membrane Science 1995;108:245.
[42] Ataka M, Sasaki K. Journal of Membrane Science 1982;11:11.
[43] Vrentas JS, Duda JL. AIChE Journal 1979;25:1.
[44] Duda JL, Vrentas JS, Ju ST, Liu HT. AIChE Journal 1982;28:279.
[45] Zielinski JM, Duda JL. AIChE Journal 1992;38:405.
[46] Vrentas JS, Duda JL, Ling H-C. J Polym Sci, Polym Phys Ed 1984;22:459.
[47] Sugden S. J Chem Soc 1927;1927:1786.
[48] Lide DR, editor. Handbook of chemistry and physics, 71st ed. Boca Raton, FL: CRC Press, 1990.
[49] Ferry JD. Viscoelastic properties of polymers, 2nd ed. New York: John Wiley, 1960.
[50] Lim GBA, Lloyd DR. Polymer Engineering and Science 1993;33:513.
[51] McAdams WH. Heat transmission, 3rd ed. New York: McGraw-Hill, 1954.
[52] Bird RB, Stewart WE, Lightfoot EN. Transport phenomena, 38th ed. New York: John Wiley, 1960.
[53] Perry RH, Green DW, Maloney JO, editors. Perry's chemical engineering handbook, 6th ed. New York: McGraw-Hill, 1984.
[54] Reid RC, Prausnitz JM, Sherwood TK. The properties of gases and liquids, 3rd ed. New York: McGraw-Hill, 1977.
[55] Lide DR, editor. Handbook of organic solvents. Boca Raton, FL: CRC Press, 1995.
[56] Chiu J, Fair PG. Thermochimica Acta 1979;34:267.
[57] Wilkinson RW, Dole M. Journal of Polymer Science 1962;58:1089.
[58] Brandrup J, Immergut EH, editors. Polymer handbook, 3rd ed. New York: John Wiley, 1989.
[59] McGuire KS, Laxminarayan A, Lloyd DR. Polymer 1994;35:4404.